



Originally published as:

Amit, H., Korte, M., Aubert, J., Hulot, G. (2011): The time-dependence of intense archeomagnetic flux patches. - Journal of Geophysical Research, 116, B12106

DOI: [10.1029/2011JB008538](https://doi.org/10.1029/2011JB008538)

# The time-dependence of intense archeomagnetic flux patches

Hagay Amit<sup>1,\*</sup>, Monika Korte<sup>2</sup>, Julien Aubert<sup>3</sup>, Catherine Constable<sup>4</sup>,  
Gauthier Hulot<sup>5</sup>

September 21, 2011

<sup>1</sup> CNRS UMR 6112, Université de Nantes, Laboratoire de Planétologie et de Géodynamique,  
2 rue de la Houssinière, Nantes, F-44000, France

<sup>2</sup> Helmholtz-Zentrum Potsdam, Deutsches GeoForschungsZentrum, Telegrafenberg, D-14473  
Potsdam, Germany

<sup>3</sup> Equipe de Dynamique des Fluides Géologiques, Institut de Physique du Globe de Paris,  
Sorbonne Paris Cité, Univ. Paris Diderot, INSU/CNRS (UMR 7154), 1 rue Jussieu, 75238  
Paris Cedex 5, France

<sup>4</sup> Institute for Geophysics and Planetary Physics, Scripps Institution of Oceanography, Uni-  
versity of California, San Diego, 9500 Gilman Drive, La Jolla, California 92093-0225, USA

<sup>5</sup> Equipe de Géomagnétisme, Institut de Physique du Globe de Paris, Sorbonne Paris Cité,  
Univ. Paris Diderot, INSU/CNRS (UMR 7154), 1 rue Jussieu, 75238 Paris Cedex 5, France

\* Corresponding author: Hagay.Amit@univ-nantes.fr (H. Amit).

*Revised (bold denotes additions, stroke denotes deletions)*

**Abstract**

20 The long-term temporal behavior of intense geomagnetic flux patches at the core-  
21 mantle boundary and the relation with lower mantle lateral heterogeneity are under de-  
22 bate. We apply an algorithm to detect centers of intense flux patches and track their  
23 time-evolution in a recent archeomagnetic field model in order to study the kinematics of  
24 such intense magnetic flux patches on millennial time scale. We find that most intense  
25 flux patches appear near the edge of the tangent cylinder. Quasi-stationary periods with  
26 small oscillations of patches occur more than drifts. Detailed comparison of the archeo-  
27 magnetic patches' behavior with that seen in numerical dynamos with tomographic heat  
28 flux boundary conditions suggests that core-mantle thermal coupling could be the cause  
29 of a statistical preference for some longitudes on the long term, which does not exclude  
30 significant time spent away from the preferred longitudes. This could explain the roughly  
31 coincident locations of high-latitude patches in the historical geomagnetic field with that  
32 of the time-average paleomagnetic field together with the much weaker patches intensity  
33 in the latter. Alternating eastward and westward drifts are also observed. The drifts are  
34 more westward than eastward, especially in the southern hemisphere, indicating that the  
35 time-average zonal core flow may also be driven by core-mantle thermal coupling. An  
36 average patch lifetime of  $\sim 300$  years is found, which we hypothesize may indicate the  
37 vortex lifetime in the outer core.

38 Keywords: Archeomagnetic field, Intense flux patches, Geodynamo, Mantle heterogeneity.

## 39 1 Introduction

40 The geomagnetic field is generated by convective motion of an electrically conducting fluid in  
41 Earth's outer core. Measurements of the geomagnetic field and its secular variation (SV) pro-  
42 vide vital constraints on the working of the geodynamo. The *gufm1* model (Jackson et al.,  
43 2000) spanning the historical period shows that the geomagnetic field at the core-mantle  
44 boundary (CMB) is characterized by high-latitude intense flux patches. These patches also  
45 seem to appear in archeomagnetic field models over millennial time scale (Korte and Con-  
46 stable, 2005; Korte et al., 2009) as well as in some paleomagnetic models representing the  
47 time-average field over the past five million years (Kelly and Gubbins, 1997). Furthermore,  
48 intense high-latitude magnetic flux patches are reproduced by numerical dynamo simulations  
49 (Christensen et al., 2010) where downwelling flow at the edge of the tangent cylinder concen-  
50 trates field lines on the outer boundary (e.g. Christensen et al., 1998).

51 If the non-zonal structures in the paleomagnetic field models are indeed robust, the most  
52 natural way to explain preferential longitudes in the steady core field is by the impact of the

53 heterogeneous mantle on the geodynamo. Numerical dynamo models with a heterogeneous  
54 heat flux outer boundary condition have indeed demonstrated that mantle control can affect  
55 the locations of intense magnetic flux patches on the CMB (Bloxham, 2002; Olson and Chris-  
56 tensen, 2002; Gubbins et al., 2007; Aubert et al., 2008). However, the time-dependence of  
57 these structures is under debate. In highly supercritical numerical dynamos with comparable  
58 thermal and magnetic diffusivities and no **volumetric** buoyancy sources or sinks, magnetic  
59 field structures are very mobile and the mantle signature appears clearly only in long-term  
60 time-averages over several magnetic diffusion times (Bloxham, 2002; Olson and Christensen,  
61 2002). In contrast, in slightly supercritical numerical dynamos with magnetic diffusivity an  
62 order of magnitude smaller than thermal diffusivity and a volumetric buoyancy source, mag-  
63 netic field locking to the boundary heterogeneity is obtained and the patches are practically  
64 stationary (Gubbins et al., 2007; Willis et al., 2007).

65 Recently Amit et al. (2010), from hereafter AAH10, studied in detail the behavior of in-  
66 tense flux patches in highly supercritical numerical dynamos with heterogeneous CMB heat  
67 flux inferred from a lower mantle seismic tomography model (Masters et al., 2000). They de-  
68 signed an algorithm to identify and track these magnetic structures. They found that the patches  
69 oscillate about preferred locations prescribed by the mantle heterogeneity with episodic drift  
70 events from one preferred location to another. The drift events were attributed to azimuthal  
71 motion of fluid downwelling structures that concentrate magnetic flux. They also observed  
72 more time-dependence in the southern hemisphere due to a stronger north-south shear in the  
73 mantle-driven zonal thermal wind there.

74 In order to improve the understanding of the dynamics of intense flux patches in Earth's  
75 core and better constrain numerical dynamo models, a characterization of the behavior of  
76 intense geomagnetic flux patches over long time periods is necessary. Time-dependent archeo-  
77 magnetic field models spanning millennial time-scales are the best available tool for that pur-  
78 pose. Constable et al. (2000) noticed that the patches in the past three millennia are mobile  
79 and not fully locked. This was confirmed in a recent study by Korte and Holme (2010), who  
80 investigated how much deviation from different time-average field configurations was required  
81 by a 7 kyr global dataset. While the existence of both northern and southern hemisphere flux  
82 lobes proved compatible with the data in the time average field but not mandatory, they found

83 evidence for considerable variability of these features on shorter time scales. Dumberry and  
84 Finlay (2007) focused on azimuthal motions of Earth's magnetic field features by investigating  
85 the time-dependent, non-zonal, high-pass filtered part of the field model *CALS7K.2* (Korte and  
86 Constable, 2005). They visualized the azimuthal motions of these features by time-longitude  
87 plots and calculated the dominant azimuthal motions at each latitude using a technique based  
88 on the Radon transform (Finlay and Jackson, 2003). They attributed most of the azimuthal  
89 motions to the mobility of the high-latitude intense flux patches in the northern hemisphere.  
90 Wardinski and Korte (2008) inverted the same field model and SV for the flow responsible for  
91 such changes at the top of the core. Their flow solutions represent 200-years time-averages  
92 (rather than snapshots) expanded up to degree 5, reflecting the limited temporal and spatial  
93 resolution of the archaeomagnetic field model. ~~Despite these cautionary measures,~~ Such inver-  
94 sions might be severely biased by uncertainties in the archeomagnetic SV.

95 This paper complements the previous ones by using a different approach and focusing on  
96 the dominant geomagnetic flux patches often found at high-latitudes. Here we apply the algo-  
97 rithm developed by AAH10 to the recent *CALS3k.3* archeomagnetic field model spanning the  
98 past three millennia to assess the behavior of the patches at the CMB. Thanks to a significantly  
99 increased data base, this model based on spherical harmonics in space and cubic B-splines in  
100 time exhibits higher resolution than its predecessors *CALS3k.1* (Korte and Constable, 2003)  
101 and *CALS3k.2* (Korte and Constable, 2005). Particularly the southern hemisphere resolution  
102 has increased, although the amount of data from the northern hemisphere still dominates. The  
103 model is expanded to spherical harmonic degree 10 in space with a 10 year knot-point spacing  
104 of the splines, but the actual resolution is significantly lower. Archeo- and paleomagnetic data  
105 contain large uncertainties, both in the magnetic data themselves and in the age determination.  
106 Regularizations in both space and time have been applied in the modeling to trade off the fit to  
107 the data against what is assumed to be a realistic and robust amount of structure, based on the  
108 comparison of geomagnetic power spectra. We use the full field model to extract the kinemat-  
109 ics of intense flux patches, including quasi-stationary periods. Our analysis enables tracking  
110 the 2D trajectory of the patches, i.e. both azimuthal and meridional motions. Analysis of the  
111 timeseries of patches coordinates allows quantifying the relative periods in which the patches  
112 are quasi-stationary or drifting, and their average and maximum lifetimes.

113 The outline of the paper is as follows. In section 2 we recall the method of AAH10 for  
 114 identifying and tracking intense patches on timeseries of snapshots. We refine their algorithm  
 115 for compatibility with the larger scale archeomagnetic field models. In section 3 we present  
 116 the results of our analysis. Comparison with previous studies, geophysical implications and  
 117 consequences for data reliability assessment are discussed in section 4. We summarize our  
 118 main findings in section 5.

## 119 2 Method

120 Following the principles of the *connected component labeling* method previously used for  
 121 detecting plumes in mantle convection simulations (Labrosse, 2002), AAH10 identified intense  
 122 patches in images from numerical dynamos by searching grid points where the absolute radial  
 123 magnetic field  $B_r$  on the outer boundary is larger than a critical threshold

$$124 \quad |B_r(\phi, \theta)| > f_b |B_r(\phi, \theta)|_{max} \quad (1)$$

125 where  $\phi$  and  $\theta$  are longitude and co-latitude spherical coordinates respectively. For the in-  
 126 stantaneous small-scale dynamo field, AAH10 set  $f_b = 0.6$ . For the large-scale time-average  
 127 fields, however, they used larger fractional values in order to adjust to the larger length-scales  
 128 and different zonal components in the time-average maps. The identified extreme points were  
 129 then grouped based on the spherical distance between one extreme point to another. Once all  
 130 extreme points were assigned to a given group, a center of mass was calculated for each group.  
 131 These centers of mass represent centers of intense flux patches.

132 We use the recent *CALS3k.3* archeomagnetic field model of Korte et al. (2009) **with a grid**  
 133 **size of  $5^\circ$  in longitude and latitude**. The snapshots in this lower resolution heavily damped  
 134 field model resemble in terms of spatial scales the time-average dynamo fields. A low  $f_b$   
 135 value is therefore prone to produce large connectivity along high-latitude belts and therefore  
 136 biased patch locations in some snapshots. A large  $f_b$  value, however, might leave some patches  
 137 unidentified. We therefore use the non-zonal field  $B_r^{nz}$  to break the connectivity between the  
 138 patches. Together with criterion (1), we also require

$$139 \quad |B_r^{nz}(\phi, \theta)| > f_{nz} |B_r^{nz}(\phi, \theta)|_{max} \quad (2)$$

140 restricting criterion (2) for normal polarity flux only.

141 The identification method is demonstrated in Fig. 1 with an arbitrary snapshot from  
142 *CALS3k.3* for  $f_b = 0.7$  and  $f_{nz} = 0.2$ . The identified intense points (Fig. 1a) are connected in  
143 the northern hemisphere through the polar region, so criterion (1) alone would cause erroneous  
144 patch location there. The identified normal polarity non-zonal points (Fig. 1b) readily separate  
145 the northern hemisphere lobes, but include many weak (mostly low-latitude) features in both  
146 hemispheres. The combination of the two criteria (Fig. 1c) results in a satisfactory detection  
147 of the centers of mass of the intense flux patches (Fig. 1d).

148 *Fig. 1*

149 Tracking of patches from one snapshot to the next is performed as in AAH10. Two patches  
150 in consecutive snapshots are labeled as the same patch if the spherical distance between them  
151 is smaller than a critical value that corresponds to an azimuthal distance  $\delta^c = \omega^e \Delta t$ , where  
152  $\omega^e \sim 0.2^\circ/yr$  is used as an upper bound longitudinal drift value based on inferred low-latitude  
153 fast drifting geomagnetic features (Bloxham and Jackson, 1991) and  $\Delta t$  is the time step.

154 An analysis of the timeseries is performed following AAH10. First, we calculate the time-  
155 derivatives of the longitudes of the intense flux patches. Semi-stationary periods termed 'St'  
156 are characterized by small time-derivatives whereas drifts are characterized by large time-  
157 derivatives, with the threshold being  $\delta^c/2\Delta t = \omega^e/2$ . Integrated amounts of time of east-  
158 ward and westward drifts are denoted by 'Ea' and 'We' respectively. The absolute rms drift  
159 rates (without distinguishing east or west) are also reported. Second, we quantify the time-  
160 dependence of the patches by their average and maximum lifetimes  $\tau_a$  and  $\tau_m$ . Unlike AAH10,  
161 we avoid reporting probabilities of patches to be in a vicinity of a time-average patch because  
162 the time-average archeomagnetic field is expected to differ from the true long-term time-  
163 average field and calculating such probabilities would clearly be biased to large values. All  
164 quantities are given for each hemisphere separately. The results of the synthetic analysis are  
165 summarized in Table 1.

### 3 Results

We first examine the locations of intense magnetic flux patches in time-average field models. In Fig. 2a we applied our method for the time-average archeomagnetic field between -1000 to 1850. For comparison, Figs. 2b and c show the time-average paleomagnetic field models of Kelly and Gubbins (1997) and Johnson and Constable (1995) respectively. The identification method using the non-zonal criterion proves useful especially for the latter which has a very dominant axial dipole component. In this model indeed, if we only relied on criterion (1), patches would be falsely identified very close to the geographical poles. Instead, the non-zonal criterion enables identifying ridges that correspond to non-zonal deviations.

*Fig. 2*

Despite the very large time disparity, the locations of the patches in the time-average archeomagnetic and paleomagnetic field models display some similarity, although they also display some significant differences. The time-average archeomagnetic field shows two intense patches in the northern hemisphere and one in the southern hemisphere, all at high-latitudes near the edge of the tangent cylinder (Fig. 2a). The paleomagnetic field model of Kelly and Gubbins (1997) also exhibits two patches in somewhat similar locations in the northern hemisphere and only one patch in the southern hemisphere (Fig. 2b). In contrast, the paleomagnetic field model of Johnson and Constable (1995) has two patches in each hemisphere.

The sensitivity of the results to the choice of the critical intensity threshold is examined by considering timeseries and synthetic analysis with  $f_b = 0.7$  and  $f_b = 0.8$ . Comparison of Figs. 3 and 4 and their corresponding values in Table 1 shows that for larger  $f_b$  fewer patches are identified. However, the main trends and statistics are overall weakly dependent on the choice of  $f_b$ .

*Fig. 3*

*Fig. 4*

*Table 1*

A movie of the identified intense flux patches spanning the period -1000 to 1850 with

193  $f_b = 0.75$  is given in *CALS3k.3.gif* (diamonds mark instantaneous patches, asterisks denote  
194 the time-average locations of the patches in the paleomagnetic field model of Kelly and Gub-  
195 bins, 1997). Fig. 5 shows the corresponding timeseries of the patch coordinates in each hemi-  
196 sphere. We also visualize in Fig. 6 the corresponding polar views of the patch trajectories in  
197 each hemisphere (each patch is denoted by the same color in Figs. 5 and 6). Figs. 5 and 6  
198 clearly highlight the lower data sampling of the archeomagnetic field model in the southern  
199 hemisphere.

200 *Fig. 5*

201 *Fig. 6*

202 To compare these results with those previously obtained by AAH10 with numerical dy-  
203 namo models, we repeat our analysis by using a larger time step of  $\Delta t = 150$  yrs (Table 1)  
204 to match the temporal data density of the dynamo models. Fig. 7 compares the timeseries of  
205 the northern hemisphere longitude of the archeomagnetic field with corresponding timeseries  
206 of 3000 years intervals from case *Tolr* of AAH10 (which most resembles the statistics of the  
207 archeomagnetic field model, see Table 2). Note that time in the numerical dynamo models  
208 has been re-scaled compared to the original scaling used in AAH10. This is justified in sec-  
209 tion 4 where the comparison between the behavior of patches in the archeomagnetic field and  
210 numerical dynamos is discussed.

211 *Fig. 7*

212 We end the analysis of the archeomagnetic field model at 1850 and complete the temporal  
213 coverage with the higher resolution historical geomagnetic field model *gufm1* derived from  
214 direct measurements (including intensity) for the period 1840-1990. The movie *gufm1.gif* and  
215 Fig. 8 demonstrate that the method performs adequately for the historical model as well. Note  
216 that the patches identified in the beginning of the historical period below North America, cen-  
217 tral Asia and southeast Pacific (Fig. 9) also appear at the end of the archeomagnetic period  
218 (Fig. 5), so the two geomagnetic field models exhibit continuity in the behavior of the patches.  
219 The 150-years period is very short for tracking significant time variability (Fig. 9). Between  
220 1840-1915 two high-latitude patches in the northern hemisphere and one in the southern hemi-  
221 sphere are present. In 1920 another high-latitude southern hemisphere patch is detected. In

222 1935 a low-latitude patch below Africa emerges. These five patches remain until 1985. In  
223 1990 one high-latitude southern hemisphere structure weakens and loses its status as a patch.

224 *Fig. 8*

225 *Fig. 9*

## 226 4 Discussion

227 We begin by comparing our results with previous studies that used different approaches to  
228 analyze the archeomagnetic field. Dumberry and Finlay (2007) found coherent azimuthal mo-  
229 tions in the northern hemisphere, but practically none in the southern hemisphere, arguing that  
230 the low resolution of the archeomagnetic field model there prevents detecting non-zonal fea-  
231 tures. We also identify many fewer patches in the southern hemisphere, although some south-  
232 ern hemisphere patches are nevertheless detected. It is important to recall that the *CALS3k.3*  
233 archeomagnetic field model used here contains more data and spatial structure, especially in  
234 the southern hemisphere, than the model *CALS3k.2* used by Dumberry and Finlay (2007). The  
235 direction of drift in our analysis alternates between eastward and westward, in agreement with  
236 Dumberry and Finlay (2007) and with Wardinski and Korte (2008). The magnitude of  $\sim 0.2$   
237  $^{\circ}/\text{yr}$  drift rates in our results is again in agreement with the rates reported by Dumberry and  
238 Finlay (2007).

239 Interestingly, based on longitudinal cross-correlation, Wardinski and Korte (2008) found  
240 in some periods opposing trends in the northern/southern hemispheres. **Dumberry and Blox-**  
241 **ham (2006) also argued that the equatorial symmetry is broken on millennial timescales.**  
242 **This is** in contradiction to equatorially-symmetric columnar flow that is thought to prevail in  
243 Earth's core on shorter timescales due to the expected dominance of rotational effects (Busse,  
244 1975; Olson et al., 1999; Jault, 2008; Pais and Jault, 2008). A pair of prominent intense flux  
245 patches in both hemispheres near  $90^{\circ}W$  (Fig. 5) is possibly the surface expression of columnar  
246 flow. To test this hypothesis, we focus on periods in which both patches are simultaneously  
247 present in Fig. 5. Between -800 to -600 and between -50 to 100 the northern patch moves east-  
248 ward, whereas the southern generally moves westward. Between 1250 to 1850 the northern

249 patch drifts westward, whereas the southern alternates between eastward and westward mo-  
250 tions. Overall, these results do not support equatorial symmetry in the kinematics of intense  
251 flux patches. It is worth stressing, however, that the kinematics of the high-latitude intense  
252 flux patches does not necessarily reflect core flow, but could alternatively result from wave  
253 propagation (**Braginsky, 1972, 1974; Braginsky and Burlatskaya, 1979; Finlay and Jack-**  
254 **son, 2003**) or a combined effect of magnetic field advection and diffusion (**Bloxham, 1986;**  
255 **Bloxham and Gubbins, 1986; Amit and Christensen, 2008; Chulliat and Olsen, 2010**).  
256 AAH10 argued that the drift of the patches in their dynamo models corresponds to azimuthal  
257 propagation of fluid downwelling structures that concentrate the magnetic field on the CMB.  
258 Therefore caution should be taken in interpreting lack of equatorial symmetry in patches tem-  
259 poral behavior as lack of equatorial symmetry in core flow.

260 The oscillatory motion of patches around a preferred location (Figs. 5 and 6) may be related  
261 to the phenomenon of archeomagnetic jerks, which are defined as sharp regional directional  
262 variations and intensity maxima in the archeomagnetic field (Gallet et al., 2003). Dumberry  
263 and Finlay (2007) speculated that archeomagnetic jerks occur when intense patches change  
264 the direction of their azimuthal oscillation. The occurrence times of archeomagnetic jerks  
265 determined from French archeomagnetic data have been summarized by Gallet et al. (2003)  
266 as approximately -800, 200, 800, 1400 and perhaps 500 and 1600. Comparison of these times  
267 with the movement of northern hemisphere flux lobes from our analysis (Fig. 5) does not show  
268 a systematic relation between archeomagnetic jerks and flux patches directional change of  
269 motion. The proposed times of archeomagnetic jerks seem to coincide with times of significant  
270 intensification or weakening of regional magnetic flux, when our detection method respectively  
271 begins or ends classifying the features as intense flux patches. The emergence or disappearance  
272 of a patch could thus be related to archeomagnetic jerks, possibly by contributing to build the  
273 hemispherical asymmetry of the field (Gallet et al., 2008).

274 We now turn to compare the behavior of the patches in the archeomagnetic field and in the  
275 numerical dynamos investigated by AAH10 (Fig. 7). As already noted, this comparison re-  
276 quires appropriate re-scaling of the time in the simulations of AAH10. Re-dimensionalization  
277 of time in numerical dynamos is indeed non-unique (Christensen and Wicht, 2007). AAH10  
278 used the magnetic diffusion time to re-scale time in their dynamo models. However, as recently

279 emphasized by Lhuillier et al. (2011), re-scaling dynamo model time by using secular variation  
280 timescales (Hulot and LeMouél, 1994) may be much more appropriate for comparisons with  
281 geomagnetic observations. Such re-scaling amounts to introducing a factor of  $Rm/Rm^e$  to  
282 the time used by AAH10 (Christensen and Tilgner, 2004). Using  $Rm^e = 760$  for Earth's core  
283 (Christensen and Tilgner, 2004, taking into account the definition of  $Rm$  used by AAH10) we  
284 obtain in Table 2 the same order of magnitude of drift rates and approach similar average life-  
285 times in the archeomagnetic field studied here and in the numerical dynamo models of AAH10.  
286 Case *T0lr* of AAH10 is closest in its  $\tau_a$  value to the archeomagnetic field, so we compare in-  
287 tervals of 3000 (re-scaled) years from this model with the analysis of the archeomagnetic field  
288 (see Fig. 7).

289 Our analysis shows that the archeomagnetic field shares some common features with the  
290 field produced by the tomographic numerical dynamos of AAH10. The patches in the archeo-  
291 magnetic field model appear near the edge of the tangent cylinder. One exception is a patch  
292 below equatorial western Pacific between 350 to 500 (~~purple~~ **orange** line in Fig. 5b). This  
293 patch could be related to the intense low-latitude flux patches observed in the historical field  
294 (Jackson, 2003), one of which below Africa is classified as intense by our algorithm (Figs. 8  
295 and 9). Even though our analysis reveals somewhat less mobility in the archeomagnetic field  
296 models than in the numerical dynamos (see larger  $St$  values in Table 1 than in Table 2), Fig. 7  
297 shows that the dynamo models can exhibit some periods with similar behavior characterized  
298 by intense patches also residing away from their long term time-average coordinates. Several  
299 archeomagnetic patches in Fig. 7a oscillate about the time-average paleomagnetic flux patch  
300 below north America (Fig. 2b), whereas the other patches are relatively distant from the Asian  
301 paleomagnetic patch. A similar behavior is seen in case *T0lr* of AAH10 during the zoom-in of  
302 Fig. 7b, where intense patches are often found in between the preferred long term time-average  
303 locations. At other times (e.g. in Fig. 7c) these patches appear to be near their time-average  
304 locations, just like over the past centuries the geomagnetic field patches locations appear near  
305 the time-average paleomagnetic flux patches seen in the northern hemisphere (Fig. 9). These  
306 observations support a statistical behavior proposed by AAH10 in which locations of high-  
307 latitude patches roughly coincide with that of the time-average paleomagnetic field while the  
308 latter appears to be much weaker.

309 Finally, it is worth pointing out that in the archeomagnetic field westward drift occurs more  
310 often than eastward. Moreover, the net drift is much more negative (i.e. more westward) in  
311 the southern hemisphere than in the northern. Although the southern hemisphere contains  
312 fewer identified patches (probably due to lower data sampling and resolution there), the few  
313 drift events are often westward (see black curve between -900 to -600 and ~~turquoise~~ **purple**  
314 curve between 0 to 250 in Fig. 5b), whereas the northern hemisphere is more balanced (Fig.  
315 5a). The hemispheric dichotomy in the net drift is in agreement with time-average core flow  
316 models inferred from inversions of geomagnetic SV data (Pais and Hulot, 2000; Amit and  
317 Olson, 2006) and supports the speculation of AAH10 that mantle-driven thermal wind may  
318 cause stronger time-dependence of patches and weaker paleomagnetic patches in the southern  
319 hemisphere.

320 In contrast to the results of AAH10, no patch is observed completing a full drift from one  
321 preferred location to another. Zoom-ins of the dynamo models also rarely show a full drift  
322 from one preferred location to another within a period of 3000 years, but a tendency for such  
323 a mobility can sometimes be identified (see e.g. Fig. 7d). In addition, the average lifetime of  
324 a patch  $\tau_a$  is longer in the southern hemisphere than in the northern, again in contrast with the  
325 findings of AAH10. The latter discrepancy could be due to low archeomagnetic data resolution  
326 in the southern hemisphere.

327 It is worth-while comparing the average lifetime  $\tau_a \sim 300$  years with other analyses of  
328 archeomagnetic field models and with some theoretical expected values. Dumberry and Fin-  
329 lay (2007) found that a period of about 100 years is required to change the azimuthal drift  
330 direction, **while the duration of a drift event is about a few hundred years.** Wardinski and  
331 Korte (2008) found an average dominant period of 800 years in their inverted core flows. **The**  
332 **study of Dumberry and Bloxham (2006), which tried to relate zonal flows reconstructed**  
333 **from archeomagnetic field models with length of day variations, also provide a timescale**  
334 **of approximately 800 years for drift events.** AAH10 argued that the time-dependence of  
335 intense magnetic flux patches is related to the motion of fluid downwelling structures that con-  
336 centrate magnetic flux. Vortices may either split when entering a shear zone, or merge when  
337 approaching other vortices. The magnetic field passively responds by splitting and merging  
338 with the vortex evolution. If that is the case, the average lifetime of  $\tau_a \sim 300$  years may be

339 related to vortex lifetime in the outer core.

## 340 **5 Summary**

341 Identifying and tracking intense archeomagnetic field structures provides insight into the work-  
342 ing of the geodynamo over millennial timescales. Here we applied the method of AAH10 on  
343 the recent field model *CALS3k.3*. As in the historical (e.g. *gufm1*) and some paleomagnetic  
344 (e.g. Kelly and Gubbins, 1997) field models, we also find that intense flux patches reside at  
345 high-latitudes close to the tangent cylinder. The patches usually oscillate about some longi-  
346 tudes rather than exhibit strictly monotonous drifts. The direction of the motions alternate  
347 between eastward and westward, but more westward drift is observed, especially in the south-  
348 ern hemisphere. The latter result is in agreement with some core flow inversions from the  
349 historical geomagnetic SV (Pais and Hulot, 2000; Amit and Olson, 2006) and numerical dy-  
350 namos with tomographic boundary conditions (AAH10), indicating that the **pattern of the**  
351 zonal core flow is possibly ~~driven~~ **influenced** by lower mantle heterogeneity.

352 In this study we argue that the nature of time-dependence of high-latitude intense geomag-  
353 netic flux patches inferred from archeomagnetic field models is in agreement with the same  
354 scenario proposed before by AAH10 based on numerical dynamo models. The temporal vari-  
355 ability of these patches is comprised of statistically longer periods near preferred locations  
356 represented by the long term time-average paleomagnetic field, providing some likelihood for  
357 the present geomagnetic flux patches to correlate with the paleomagnetic patches. However,  
358 the patches are mobile enough and can be found at times far from these preferred locations,  
359 hence resulting in the weaker non-dipole signature in the paleomagnetic field with respect to  
360 the present geomagnetic field.

361 As in previous studies of archeomagnetic field models (e.g. Dumberry and Finlay, 2007;  
362 Wardinski and Korte, 2008), our analysis clearly suffers from low statistical sampling, both  
363 in space and in time. **It is therefore possible, for example, that in some cases appearances**  
364 **and disappearances of patches might be caused by incomplete data distribution, although**  
365 **such biases seem unlikely because several sediment records span the whole time interval.**

366 To confirm the robustness of our findings, higher resolution archeomagnetic field models are  
367 required. Especially in the southern hemisphere, more records are needed to resolve more  
368 detailed structure. Improving archeomagnetic field models clearly poses a high-priority chal-  
369 lenge for better probing the behavior of the geodynamo.

## 370 **Acknowledgments**

371 C.C. acknowledges support from NSF grant EAR 0809709. **We thank Mathieu Dumb-**  
372 **erry and an anonymous reviewer for their constructive comments that improved this**  
373 **manuscript.** This is IPGP contribution xxxx.

## References

- 375 Amit, H., Aubert, J., Hulot, G., 2010. Stationary, oscillating or drifting mantle-driven geomag-  
376 netic flux patches? *J. Geophys. Res.* B07108, doi:10.1029/2009JB006542.
- 377 Amit, H., Christensen, U., 2008. Accounting for magnetic diffusion in core flow inversions  
378 from geomagnetic secular variation. *Geophys. J. Int.* 175, 913–924.
- 379 Amit, H., Olson, P., 2006. Time-average and time-dependent parts of core flow. *Phys. Earth*  
380 *Planet. Inter.* 155, 120–139.
- 381 Aubert, J., Amit, H., Hulot, G., Olson, P., 2008. Thermo-chemical flows couple the Earth's  
382 inner core growth to mantle heterogeneity. *Nature* 454, 758–761.
- 383 Bloxham, J., 1986. The expulsion of magnetic flux from the earth's core. *Geophys. J. R. Astr.*  
384 *Soc.* 87, 669–678.
- 385 Bloxham, J., 2002. Time-independent and time-dependent behaviour of high-latitude flux bun-  
386 dles at the core-mantle boundary. *Geophys. Res. Lett.* 29, doi:10.1029/2001gl014543.
- 387 Bloxham, J., Gubbins, D., 1986. Geomagnetic field analysis - IV. Testing the frozen-flux  
388 hypothesis. *Geophys. J. R. Astr. Soc.* 84, 139–152.
- 389 Bloxham, J., Jackson, A., 1991. Fluid flow near the surface of the earth's outer core. *Rev.*  
390 *Geophys.* 29, 97–120.
- 391 Braginsky, S., 1972. Analytical description of geomagnetic field of the past and spectral anal-  
392 ysis of magnetic waves in the Earth's core. *Geomag. Aeron.* 12, 1092–1105.
- 393 Braginsky, S., 1974. Analytical description of geomagnetic field of the past and spectral anal-  
394 ysis of magnetic waves in the Earth's core II. *Geomag. Aeron.* 14, 522–529.
- 395 Braginsky, S., Burlatskaya, S., 1979. Spherical analysis of the geomagnetic field based on  
396 archeomagnetic data. *Izv. Akad. Nauk. SSSR, Fiz. zimli* 15, 891–895.
- 397 Busse, F., 1975. A model of the geodynamo. *Geophys. J. R. Astron. Soc.* 42, 437–459.

- 398 Christensen, U., Aubert, J., Hulot, G., 2010. Conditions for Earth-like geodynamo models.  
399 Earth Planet. Sci. Lett. 296, 487–496.
- 400 Christensen, U., Olson, P., Glatzmaier, G., 1998. A dynamo model interpretation of geomag-  
401 netic field structures. Geophys. Res. Lett. 25, 1565–1568.
- 402 Christensen, U., Tilgner, A., 2004. Power requirement of the geodynamo from ohmic losses in  
403 numerical and laboratory dynamos. Nature 439, 169–171.
- 404 Christensen, U., Wicht, J., 2007. Numerical dynamo simulations. In: Olson, P. (Ed.), *Treatise*  
405 *on Geophysics*. Vol. 8. Elsevier Science.
- 406 Chulliat, A., Olsen, N., 2010. Observation of magnetic diffusion in the Earth’s outer core from  
407 Magsat, Orsted and CHAMP data,. J. Geophys. Res. 115, doi:10.1029/2009JB006994.
- 408 Constable, C., Johnson, C., Lund, S., 2000. Global geomagnetic field models for the past 3000  
409 years: transient or permanent flux lobes? Philos. Trans. R. Soc. Lond. A358, 991–1008.
- 410 Dumberry, M., Bloxham, J., 2006. Azimuthal flows in the Earth’s core and changes in the  
411 length of day at millennial timescales. Geophys. J. Int. 165, 32–46.
- 412 Dumberry, M., Finlay, C., 2007. Eastward and westward drift of the Earth’s magnetic field for  
413 the last three millennia. Earth Planet. Sci. Lett. 254, 146–157.
- 414 Finlay, C., Jackson, A., 2003. Equatorially dominated magnetic field change at the surface of  
415 Earth’s core. Science 300, 2084–2086.
- 416 Gallet, Y., Genevey, A., Courtillot, V., 2003. On the possible occurrence of archeomagnetic  
417 jerks in the geomagnetic field over the past three millennia. Earth Planet. Sci. Lett. 214,  
418 237–242.
- 419 Gallet, Y., Hulot, G., Chulliat, A., Genevey, A., 2008. Geomagnetic field hemispheric asym-  
420 metry and archeomagnetic jerks. Earth Planet. Sci. Lett. 284, 179–186.
- 421 Gubbins, D., Willis, P., Sreenivasan, B., 2007. Correlation of earth’s magnetic field with lower  
422 mantle thermal and seismic structure. Phys. Earth Planet. Inter. 162, 256–260.

- 423 Hulot, G., LeMouél, J.-L., 1994. A statistical approach to the Earth's main magnetic field.  
424 *Phys. Earth Planet. Inter.* 82, 167–183.
- 425 Jackson, A., 2003. Intense equatorial flux spots on the surface of the Earth's core. *Nature* 424,  
426 760–763.
- 427 Jackson, A., Jonkers, A., Walker, M., 2000. Four centuries of geomagnetic secular variation  
428 from historical records. *Phil. Trans. R. Soc. Lond.* A358, 957–990.
- 429 Jault, D., 2008. Axial invariance of rapidly varying diffusionless motions in the Earth's core  
430 interior. *Phys. Earth Planet. Inter.* 166, 67–76.
- 431 Johnson, C., Constable, C., 1995. The time averaged geomagnetic field as recorded by lava  
432 flows over the past 5 myr. *Geophys. J. Int.* 122, 489–519.
- 433 Kelly, P., Gubbins, D., 1997. The geomagnetic field over the past 5 million years. *Geophys. J.*  
434 *Int.* 128, 315–330.
- 435 Korte, M., Constable, C., 2003. Continuous global geomagnetic field models for the past 3000  
436 years. *Phys. Earth Planet. Inter.* 140, 73–89.
- 437 Korte, M., Constable, C., 2005. Continuous geomagnetic models for the past 7 millennia ii:  
438 Cals7k. *Geochem. Geophys. Geosyst.* 6(2), Q02H16.
- 439 Korte, M., Donadini, F., Constable, C., 2009. The geomagnetic field for 0-3ka: 2. a new series  
440 of time-varying global models. *J. Geophys. Res.* 10, Q06008, doi:10.1029/2008GC002297.
- 441 Korte, M., Holme, R., 2010. On the persistence of geomagnetic flux lobes in global field  
442 models. *Phys. Earth Planet. Inter.* 182, 179–186.
- 443 Labrosse, S., 2002. Hotspots, mantle plumes and core heat loss. *Earth Planet. Sci. Lett.* 199,  
444 147–156.
- 445 Lhuillier, F., Fournier, A., Hulot, G., Aubert, J., 2011. The geomagnetic secular-variation  
446 timescale in observations and numerical dynamo models. *Geophys. Res. Lett.* 38, L09306,  
447 doi:10.1029/2011EL047356.

- 448 Masters, G., Laske, G., Bolton, H., Dziewonski, A., 2000. The relative behavior of shear  
449 velocity, bulk sound velocity, and compressional velocity in the mantle: Implications for  
450 chemical and thermal structure. In: Karato, S., Forte, A., Liebermann, R., Masters, G.,  
451 Stixrude, L. (Eds.), *Earths deep interior*. Vol. 117. AGU monograph, Washington D.C.
- 452 Olson, P., Christensen, U., 2002. The time averaged magnetic field in numerical dynamos with  
453 nonuniform boundary heat flow. *Geophys. J. Int.* 151, 809–823.
- 454 Olson, P., Christensen, U., Glatzmaier, G., 1999. Numerical modeling of the geodynamo:  
455 Mechanisms of field generation and equilibration. *J. Geophys. Res.* 104, 10383–110404.
- 456 Pais, A., Hulot, G., 2000. Length of day decade variations, torsional oscillations and inner core  
457 superrotation:evidence from recovered core surface zonal flows. *Earth Planet. Sci. Lett.* 118,  
458 291–316.
- 459 Pais, M. A., Jault, D., 2008. Quasi-geostrophic flows responsible for the secular variation of  
460 the earth's magnetic field. *Geophys. J. Int.*, doi:10.1111/j.1365–246X.2008.03741.x.
- 461 Wardinski, I., Korte, M., 2008. The evolution of the core-surface flow over the last seven  
462 thousands years. *J. Geophys. Res.* 113, doi:10.1029/2007JB005024.
- 463 Willis, P., Sreenivasan, B., Gubbins, D., 2007. Thermal core-mantle interaction: Exploring  
464 regimes for 'locked' dynamo action. *Phys. Earth Planet. Inter.* 165, 83–92.

## Figure captions

**Figure 1** Demonstration of the patches identification method for the radial field  $B_r$  of the archeomagnetic model *CALS3k.3* in year -800. (a) Intense points based on criterion (1) with  $f_b = 0.7$ ; (b) Non-zonal points based on criterion (2) with  $f_{nz} = 0.2$ ; (c) Points that pass the two criteria; (d) The identified centers of patches. Identified points in (a)-(c) are denoted by small empty diamonds; Centers of identified patches in (d) are denoted by large filled diamonds. **Solid black lines mark the latitudes where the tangent cylinder intersects the CMB.**

**Figure 2** Time-average radial magnetic field on the CMB and the identified patches. (a) The archeomagnetic model *CALS3k.3* of Korte et al. (2009) for the past three millennia; (b) The paleomagnetic model of Kelly and Gubbins (1997) for the past five million years; (c) The paleomagnetic model *LSNI* of Johnson and Constable (1995) for the past five million years. In all cases we set  $f_b = 0.75$  and  $f_{nz} = 0.2$ . Centers of identified patches are denoted by diamonds. **Solid black lines mark the latitudes where the tangent cylinder intersects the CMB.**

**Figure 3** Timeseries of the longitude (upper panel) and latitude (lower panel) of the centers of mass of the intense patches (distinguished by different colors) in model *CALS3k.3* with  $f_b = 0.7$  and  $f_{nz} = 0.2$  in the northern (a) and southern (b) hemispheres. Coordinates units are in degrees. Dashed horizontal lines denote the coordinates of the patches identified in the time-average field of Kelly and Gubbins (1997) in each hemisphere (see Fig. 2b). Dotted horizontal lines in the latitude (lower) subplots denote the tangent cylinder. As time progresses, each new color represents a new patch. For a given color, positive/negative trends correspond to eastward/westward patch drift in the longitude curves, or northward/southward in the latitude curves.

**Figure 4** Sensitivity test: As in Fig. 3 for  $f_b = 0.8$ .

**Figure 5** As in Fig. 3 for  $f_b = 0.75$ .

**Figure 6** Polar views of patches trajectories corresponding to Fig. 5. Dotted horizontal lines denote the tangent cylinder. Each patch has the same color as in Fig. 5. The locations

493 of the time-average paleomagnetic patches of Kelly and Gubbins (1997) are denoted by  
494 green diamonds.

495 **Figure 7** Comparison between *CALS3k.3* (a) and the dynamo model *T0lr* of AAH10 (b-d).  
496 In (a) the model was down-sampled to  $\Delta t = 150$  for compatibility with the sampling  
497 density in (b-d). In (b-d) time was re-scaled by  $Rm/Rm^e$  compared to the original  
498 scaling used in AAH10 (see discussion for details). Only the timeseries of the northern  
499 hemisphere longitudes are shown. The dashed lines in (a) represent the coordinates of  
500 intense flux patches in the time-average paleomagnetic field model of Kelly and Gubbins  
501 (1997), while in (b) the dashed lines are the time-average coordinates in the numerical  
502 dynamo model.

503 **Figure 8** Patches identification in the radial geomagnetic field of 1980 from *gufm1* (Jackson  
504 et al., 2000) with  $f_b = 0.8$  and  $f_{nz} = 0.2$ .

505 **Figure 9** Timeseries of the longitude (left) and latitude (right) of the centers of mass of in-  
506 tense patches (distinguished by different colors) in model *gufm1* with  $f_b = 0.8$  and  
507  $f_{nz} = 0.2$  in the northern (a) and southern (b) hemispheres. Coordinates units are in  
508 degrees. Dashed horizontal lines denote the coordinates of the patches identified in the  
509 time-average field of Kelly and Gubbins (1997) in each hemisphere (see Fig. 2b). Dot-  
510 ted horizontal lines in the latitude (right) subplots denote the tangent cylinder. As time  
511 progresses, each new color represents a new patch. For a given color, positive/negative  
512 trends correspond to eastward/westward patch drift in the longitude curves, or north-  
513 ward/southward in the latitude curves.

## Tables

$f_b$	$\Delta t$	NH								
		St	Ea	We	Ne	Rate	$\tau_a$	$\tau_m$	$N_p$	
0.7	50	83.1	2.4	14.5	-12.1	0.20	239	950	1.8	
0.75	50	84.4	2.6	13.0	-10.4	0.18	264	950	1.6	
0.8	50	88.9	1.4	9.7	-8.3	0.17	275	950	1.5	
0.75	150	84.0	8.0	8.0	0.0	0.16	525	1350	1.8	
		SH								
		St	Ea	We	Ne	Rate	$\tau_a$	$\tau_m$	$N_p$	
0.7	50	68.9	6.6	24.6	-18.0	0.19	327	900	1.2	
0.75	50	62.8	7.0	30.2	-23.2	0.18	289	900	0.9	
0.8	50	57.6	6.1	36.4	-30.3	0.18	325	850	0.7	
0.75	150	44.5	11.1	44.4	-33.3	0.15	319	900	0.9	

Table 1: Synthetic analysis of *CALS3k.3* for different  $f_b$  and  $\Delta t$  values (in all cases  $f_{nz} = 0.2$ ). The time step  $\Delta t$  is given in years. Percentage of time with semi-stationary events is denoted by 'St', percentage of time with eastward/westward drifts are denoted by 'Ea'/'We' respectively. The net drift is defined by  $Ne = Ea - We$ . The threshold distinguishing semi-stationary events from drifts is  $\omega^e/2$ . The rms values of the absolute drift rates (denoted by 'Rate') are given in  $^\circ/\text{year}$ . The average and longest lifetimes of patches  $\tau_a$  and  $\tau_m$  are given in years, **and the average number of patches per snapshot is  $N_p$** . The analysis is given for each hemisphere, with northern/southern hemispheres denoted by NH/SH respectively.

Case	NH						
	St	Ea	We	Ne	Rate	$\tau_a$	$\tau_m$
<i>T0lr</i>	43.3	23.3	32.8	-9.5	0.20	298	6099
<i>T0</i>	52.5	28.1	19.4	8.7	0.15	653	3947
<i>T0hr</i>	52.9	22.1	25.0	-2.9	0.21	654	6020
<i>T0hq</i>	53.2	22.4	24.4	-2.0	0.15	819	7892
	SH						
	St	Ea	We	Ne	Rate	$\tau_a$	$\tau_m$
<i>T0lr</i>	36.2	23.0	40.8	-17.8	0.21	251	2866
<i>T0</i>	49.7	19.9	30.4	-10.5	0.15	405	6135
<i>T0hr</i>	48.8	22.9	28.3	-5.4	0.21	590	4545
<i>T0hq</i>	40.0	19.2	40.8	-21.6	0.16	383	2885

Table 2: Synthetic analysis of the numerical dynamos timeseries from AAH10, where time is however re-scaled by  $Rm/Rm^e$  with  $Rm^e = 760$  compared to the original results of AAH10 (their Table 3). All quantities are defined as in Table 1, the threshold distinguishing semi-stationary events from drifts being also  $\omega^e/2$ .

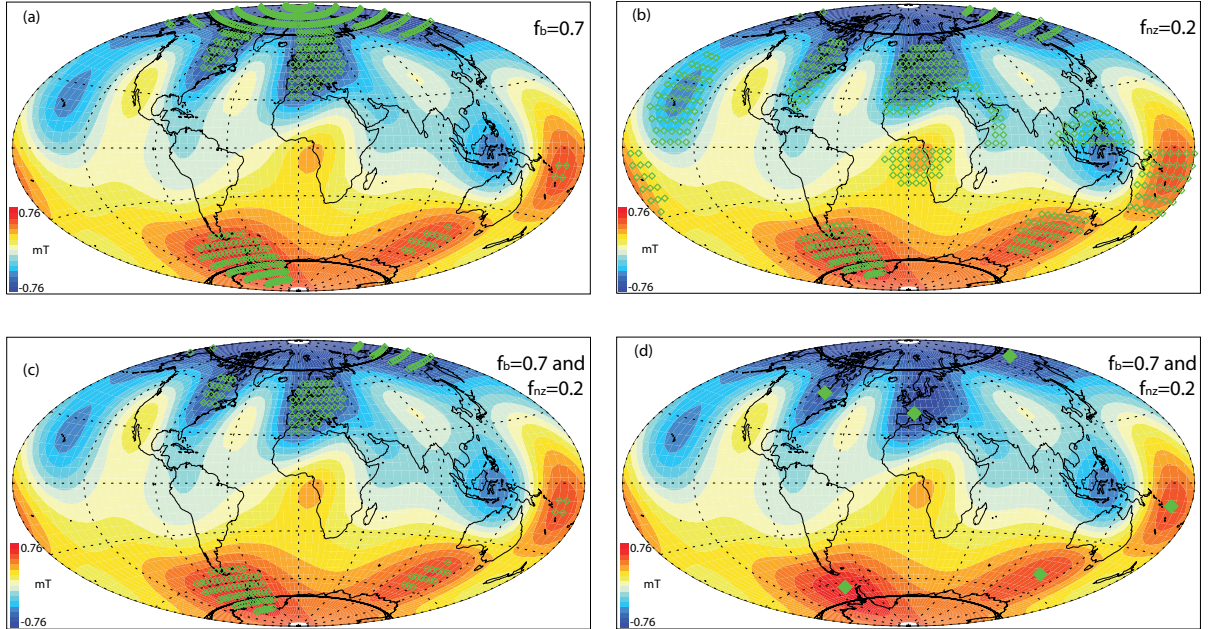


Figure 1:

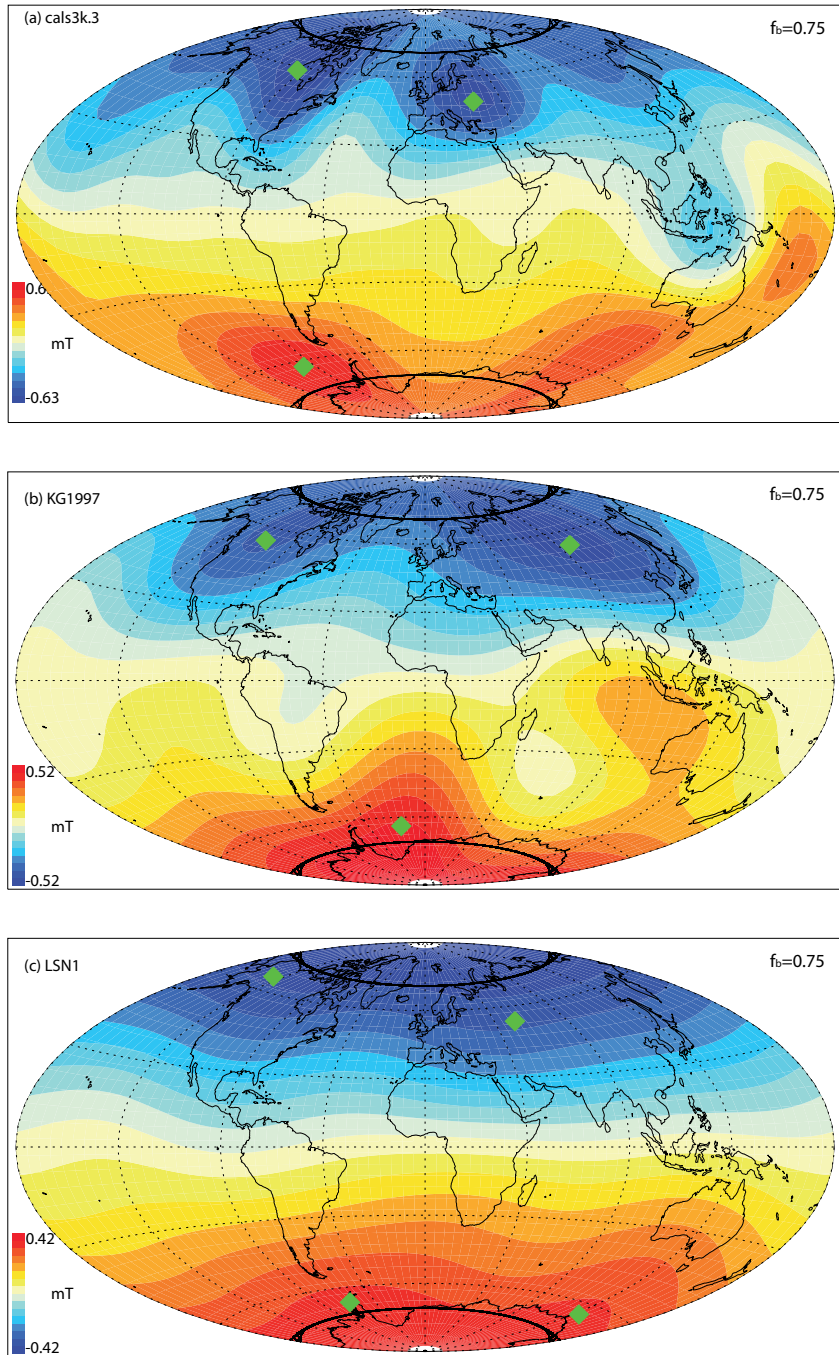


Figure 2:

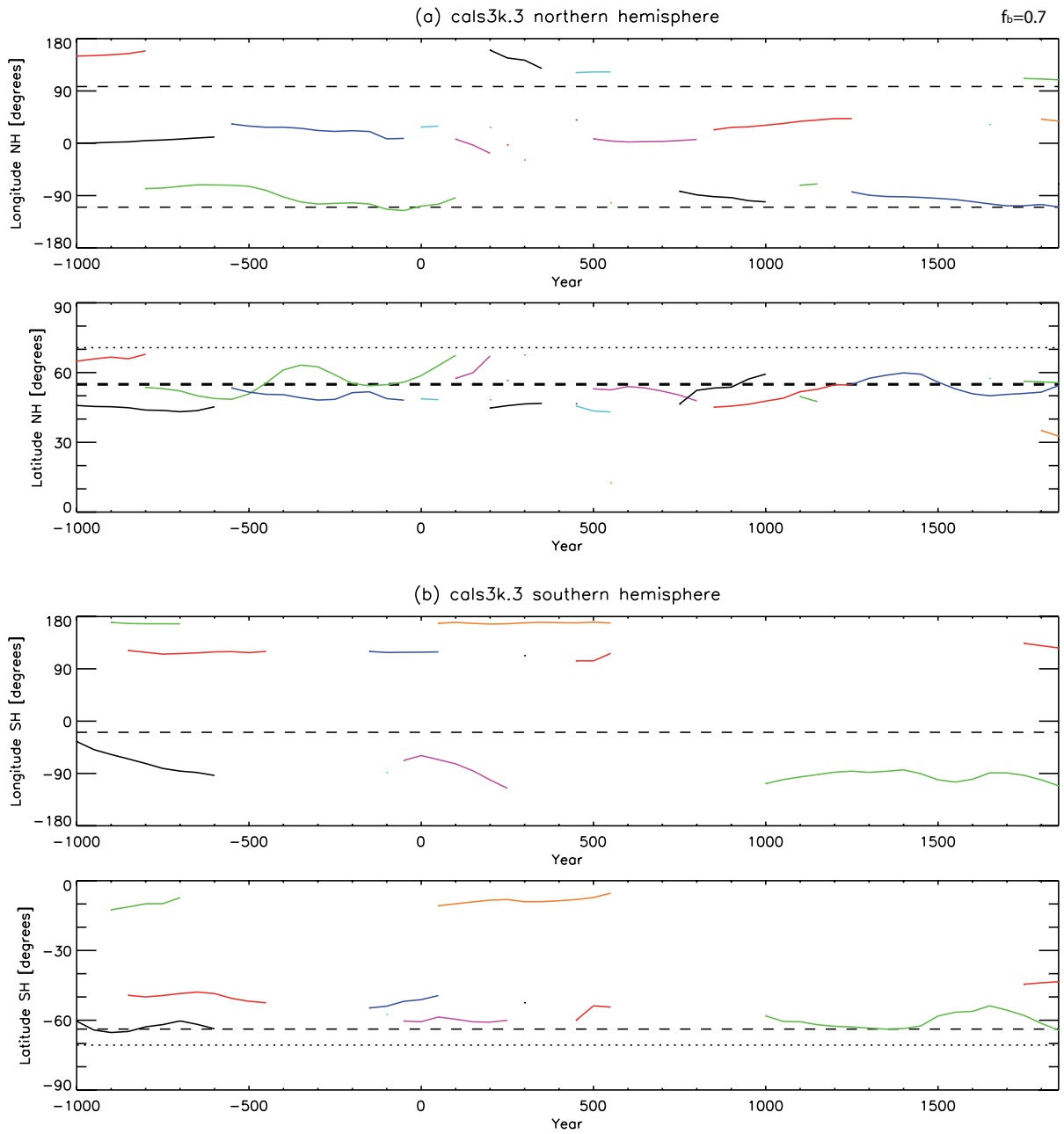


Figure 3:

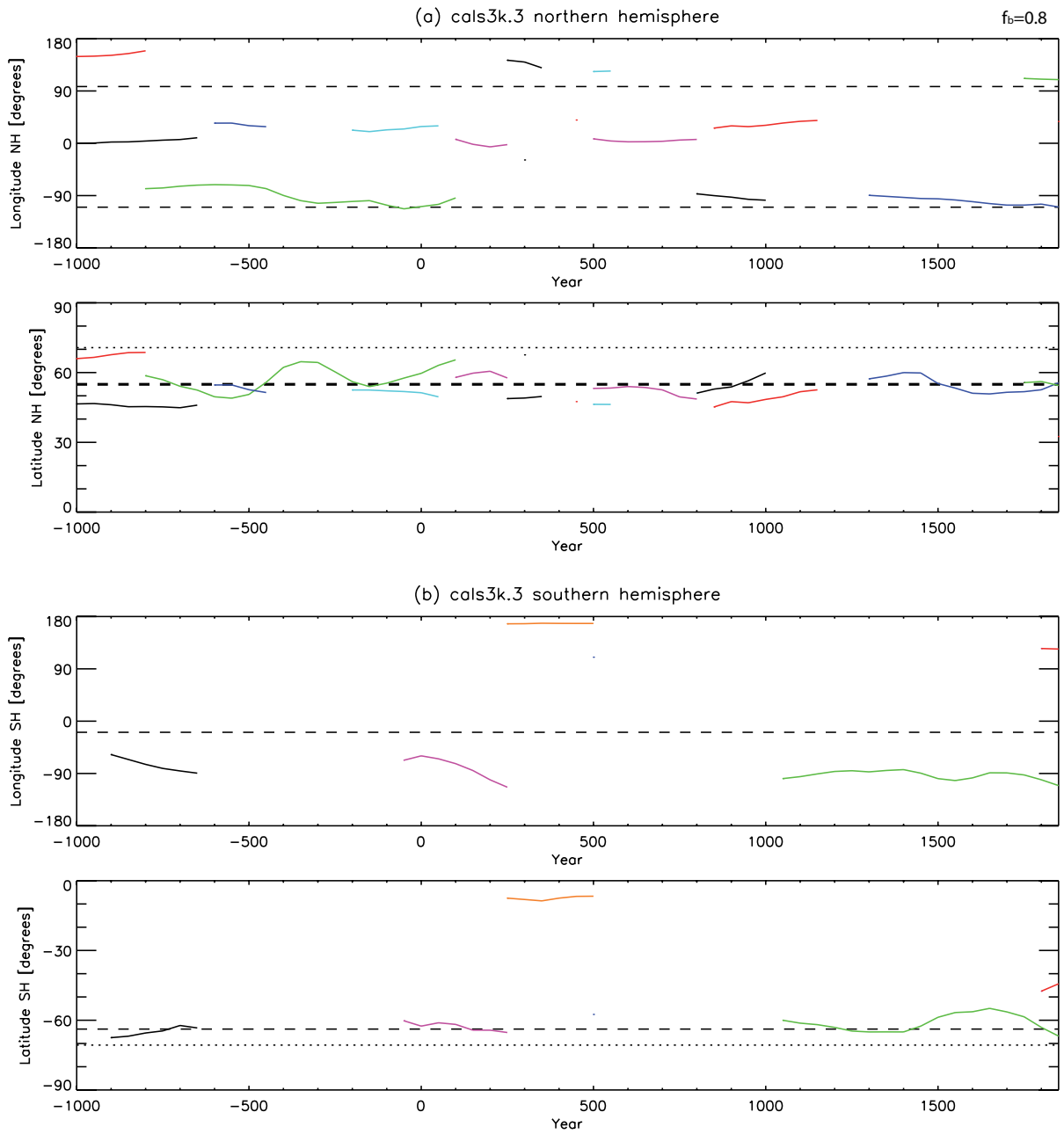


Figure 4:

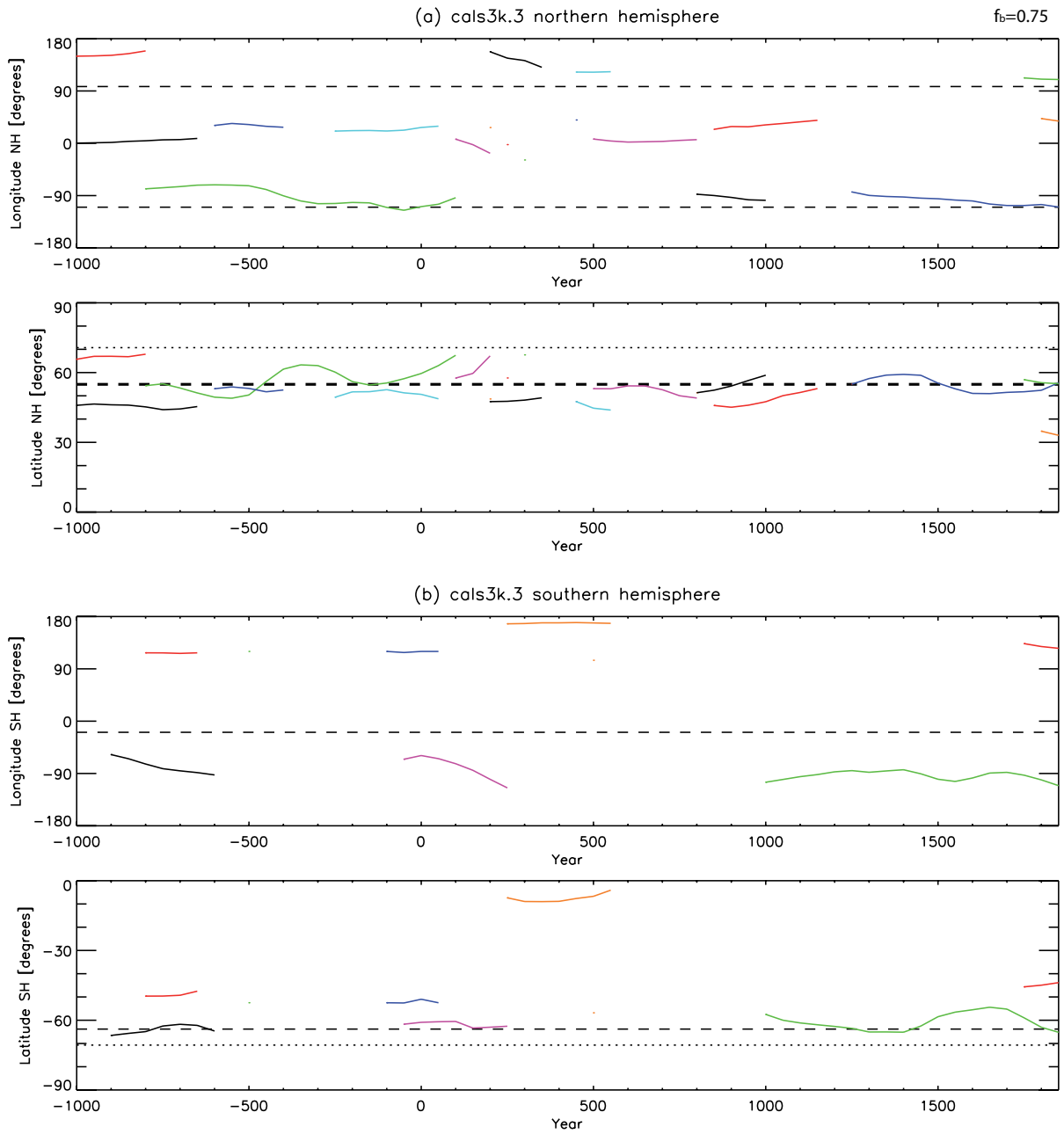


Figure 5:

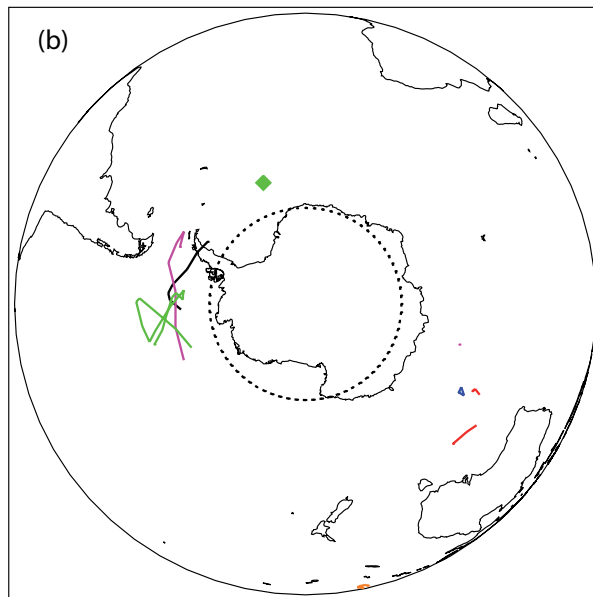
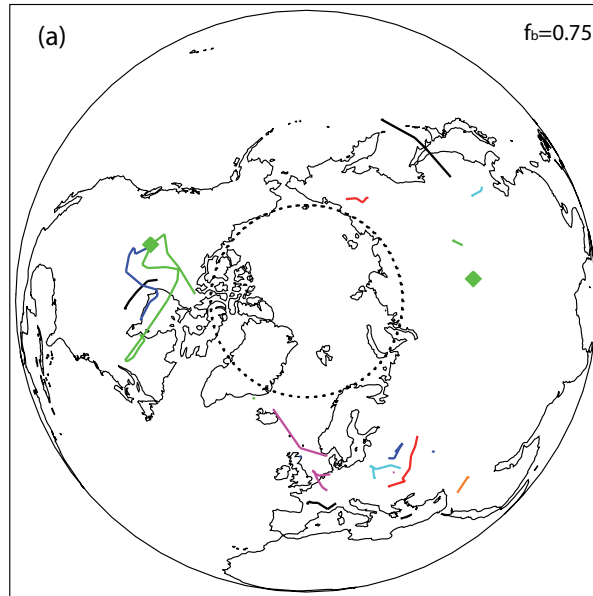


Figure 6:

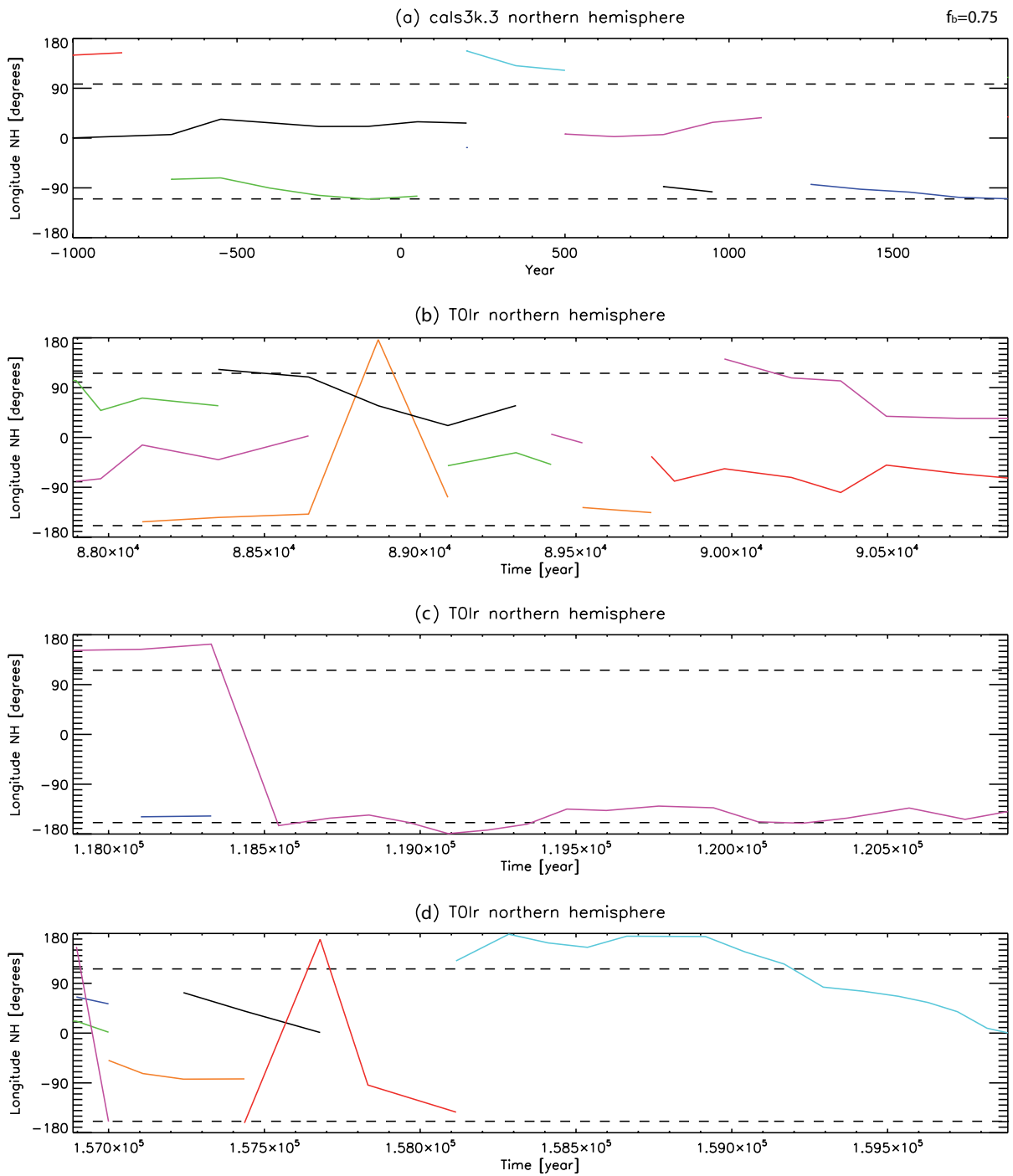


Figure 7:

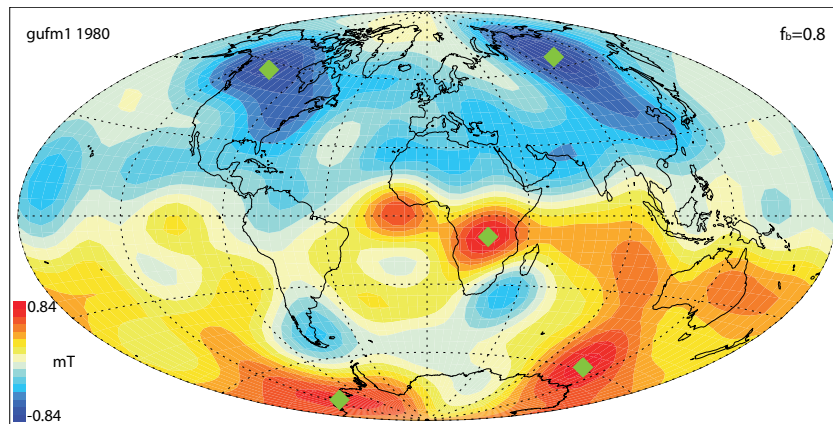


Figure 8:

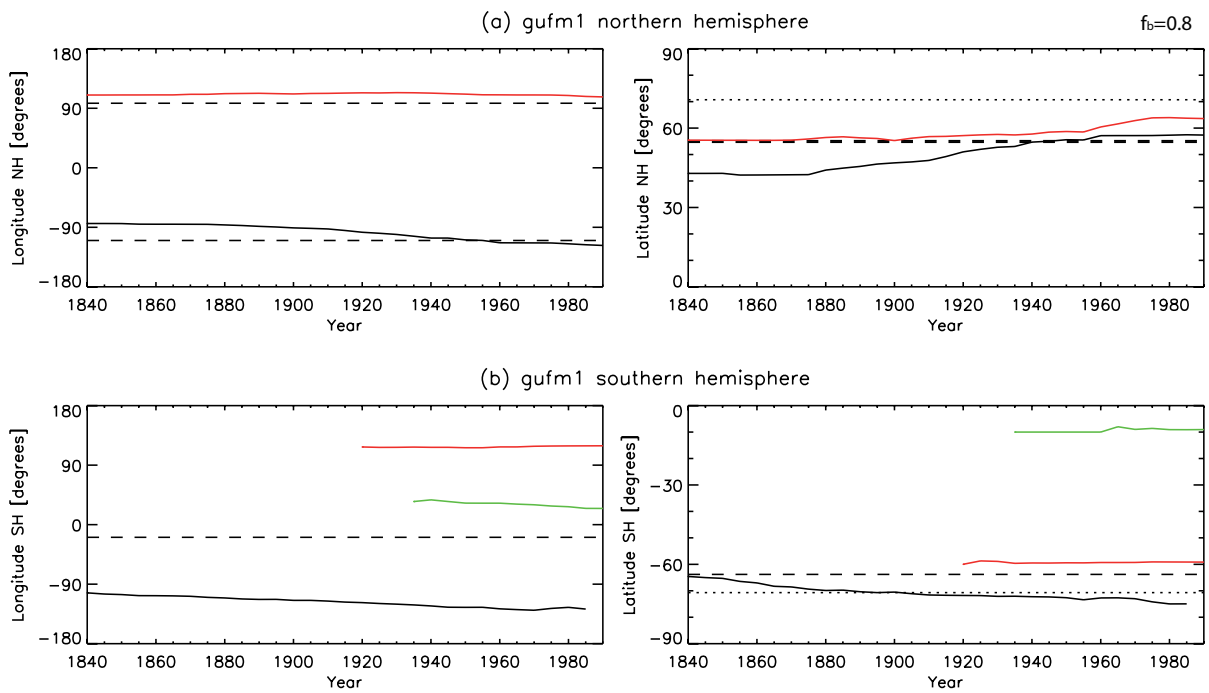


Figure 9: